International Journal of Bifurcation and Chaos, Vol. 14, No. 5 (2004) 1625–1641

STUDY OF DEGENERATE BIFURCATIONS IN MAPS: A FEEDBACK SYSTEMS APPROACH

MARÍA BELÉN D'AMICO*, JORGE L. MOIOLA and EDUARDO E. PAOLINI
Departamento de Ingeniería Eléctrica y de Computadoras
Universidad Nacional del Sur
Avda Alem 1253, B8000CPB Bahía Blanca, Argentina
**mbdamico@criba.edu.ar*

Received January 22, 2003; Revised March 26, 2003

The dynamical behavior of nonlinear maps undergoing degenerate period doubling or degenerate Hopf bifurcations is studied via a frequency-domain approach. The technique is based on a discrete-time feedback representation of the system and the application of the well-known engineering tools of harmonic balance to approximate the emerging solutions. More specifically, the results are a higher-order extension of the previous developments obtained by the authors for nondegenerate bifurcations. Two examples are included for illustration.

Keywords: Bifurcation theory; harmonic analysis; discrete-time systems.

1. Introduction

Bifurcations in discrete-time systems sometimes parallels the qualitative changes in dynamics in continuous-time systems after varying certain parameters. However, two important differences show up at a first glance: the stability domain changes from the left half-plane — for continuous-time systems — to the interior of the unit circle — for discrete-time systems, and the appearance of resonances make more complicated the analysis of the dynamics in maps. Concentrating on the group of elementary singularities in discrete-time systems, the classical bifurcations are distinguished as saddle-node, transcritical, pitchfork, period-doubling and Hopf bifurcations. The former three bifurcations are related to the presence of multiple fixed points (or period-one points) near the singularity while the last two cases are categorized in a different class. In particular, period-doubling bifurcations are characterized by the presence of period-two points in the vicinity of a period-one point whereas Hopf bifurcations consist of an invariant orbit emerging from the existing fixed point. In both cases, the original fixed point usually changes its stability at the bifurcation. For the sake of simplicity, this change will be implied in the rest of the paper, unless it is specifically noted.

Period-doubling and Hopf bifurcations have always been interesting cases of study since their appearances commonly announce the existence of other types of complex phenomena, even the presence of chaos, and help in the understanding of dynamical complexities in continuous-time systems via the so-called Poincaré map. Some of the most distinctive applications are in the field of power electronic circuits [Deane & Hamill, 1990; Tse, 1994; Aroudi *et al.*, 1999; di Bernardo & Vasca, 2000; Tse *et al.*, 2000; Mazumder *et al.*, 2001], adaptive control systems [Golden & Ydstie, 1988; Mareels & Bitmead, 1988; Frouzakis *et al.*, 1991, 1996] and population biology [Selgrade & Roberds, 1997; Dilão & Domingos, 2001]. Traditionally, these bifurcations have been analyzed by using the normal form theorem [Kuznetsov, 1995]. This theorem consists basically in the conversion of the difference equations to a typical normal form via a coordinate

transformation. Then, the conditions to characterize which type of bifurcation the system will develop are obtained from selected nonvanishing coefficients on this new representation. The main disadvantage of this procedure is the need of extensive and laborious calculations in order to reduce the system in its minimum dimension: dimension one for period-doubling bifurcation and dimension two for Hopf bifurcations.

Recently, the authors have proposed a frequency-domain methodology to compute period doubling and Hopf bifurcations in maps [D'Amico *et al.*, 2002, 2003a]. The approach is based on a discrete-time feedback representation of the system and the application of well-known engineering tools of harmonic balance via Fourier series. The bifurcations are detected via the general Nyquist stability criterion, and then a second-order harmonic balance method is used to approximate the solutions and to determine their stability. For period-doubling bifurcations, the approximation consists of a correction term, for an eventual shift in the fixed point, together with another term representing the characteristic alternation of these orbits. In the case of Hopf bifurcations, on the other hand, a rather complete expansion into the bias, the first- and second-order harmonics is performed.

In this paper, these results are extended in order to study more complex bifurcations. Towards this end, higher-order approximations of the emerging orbits and also algebraic expressions of the so-called stability indices are derived. These indices are helpful in understanding the dynamics of the nonlinear maps, especially, when they have degenerate period-doubling or degenerate Hopf bifurcations. Although these degeneracies seem to be confined and isolated in the space of system parameters, their effects are noticeable in wide regions of the parameter space and so they are worthy for classification purposes. For instance, there exists a kind of degenerate period-doubling bifurcation which announces the multiplicity of the period-two orbits and the presence of saddle-node bifurcations in the period-two branch (see [Peckham & Kevrekidis, 1991] for a derivation of the formulas using singularity theory). Analogously, a kind of degenerate Hopf bifurcation precludes the multiplicity of invariant orbits and then the presence of a saddle-node bifurcation in the invariant orbit branch [Chenciner, 1985; Shilnikov *et al.*, 2001]. Therefore, since both saddle-node structures end at the degenerate point, an accurate detection of this point and the availability of approximation formulas for local detection of the branches are useful.

The outline of the paper is as follows. In Sec. 2, the detection of bifurcations of discrete-time systems is formulated in the frequency-domain. Moreover, the critical conditions for determining the existence of strong resonance points are given. In Sec. 3, the procedure to approximate degenerate period-doubling and degenerate Hopf bifurcations is described. To illustrate the usefulness of this methodology, two examples are worked out in Sec. 4. Finally, some concluding remarks are given in Sec. 5.

2. Study of Bifurcations in the Frequency-Domain

In many situations, feedback models represent a more suitable way to study the dynamics of the systems. The classical block diagram of a discrete-time Lur'e system, shown in Fig. 1, consists of the closed-loop connection between a linear block, defined by the $m \times l$ rational transfer matrix $G(z;\mu)$, and a memoryless nonlinear part given by the function $f : \mathbf{R}^m \to \mathbf{R}^l$. In the figure, $v_k \in \mathbf{R}^l$ is the external input, $y_k \in \mathbf{R}^m$ is the output, $u_k \in \mathbf{R}^l$ is the control variable, $\mu \in \mathbf{R}^s$ is the parameter vector and z is the complex variable corresponding to the z-transform operation. In the following, it will be assumed that $v_k = \mathbf{0}$ and $f(\cdot)$ is a smooth C^{2q+1} function jointly in y_k and μ, where $2q$ will be the order of the harmonic balance approximations.

This feedback representation is not restricted to a particular kind of discrete-time systems. In fact, any state-space formulation, such as

$$\begin{aligned} x_{k+1} &= Ax_k + Bh(y_k;\mu)\,, \\ y_k &= Cx_k\,, \end{aligned} \tag{1}$$

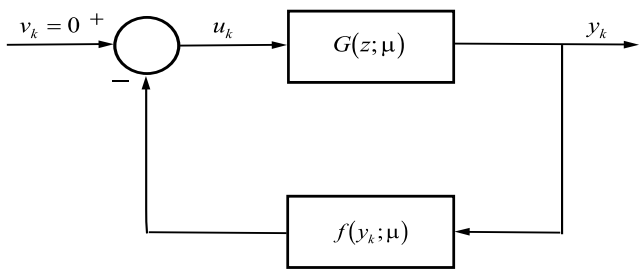

Fig. 1. A discrete-time feedback system consisting of a closed-loop connection between a transfer matrix $G(\cdot)$ and a nonlinear function $f(\cdot)$.

where $k \in \mathbf{N}$, x_{k+1}, $x_k \in \mathbf{R}^n$, $h : \mathbf{R}^m \times \mathbf{R}^s \to \mathbf{R}^l$ and the matrices $A \in \mathbf{R}^{n\times n}$, $B \in \mathbf{R}^{n\times l}$ and $C \in \mathbf{R}^{m\times n}$ may depend on μ, can be decomposed into a linear and a nonlinear part. Furthermore, many distinct but equivalent decompositions can be achieved by introducing an arbitrary matrix $D \in \mathbf{R}^{l\times m}$ (that may also depend on μ) and rewriting (1) as

$$\begin{aligned} x_{k+1} &= Ax_k + BDy_k + B[h(y_k;\mu) - Dy_k]\,, \\ y_k &= Cx_k\,. \end{aligned} \tag{2}$$

After applying the z-transform, system (2) results in a closed loop consisting of the linear subsystem

$$G(z;\mu) = C[zI - (A + BDC)]^{-1}B\,, \tag{3}$$

and the memoryless nonlinear feedback

$$f(y_k;\mu) = Dy_k - h(y_k;\mu) := -u_k\,. \tag{4}$$

In practice, matrix D is useful to obtain a simpler realization, and the fundamental results do not depend on it.

Following a similar procedure as the usual study of dynamics in the time-domain, the fixed points of a feedback model (denoted as $\hat{y}$) are given by

$$G(1;\mu)f(\hat{y};\mu) + \hat{y} = 0 \tag{5}$$

and the linearized system is defined by the open-loop matrix $G(z;\mu)J(\mu)$ where $J(\cdot)$ is the Jacobian matrix[1] $J(\mu) = D_1 f(\hat{y};\mu)$. Then, the eigenvalues λ are obtained by solving the algebraic equation

$$\begin{aligned} g_0(\lambda;z;\mu) &= \det|\lambda I - G(z;\mu)J(\mu)| \\ &= \lambda^t + a_{t-1}(z;\mu)\lambda^{t-1} + \cdots \\ &\quad + a_1(z;\mu)\lambda + a_0(z;\mu) \\ &= 0\,, \end{aligned} \tag{6}$$

where $t = \min(m,l)$ is the rank of $G(z;\mu)J(\mu)$, and $a_i(z;\mu)$ with $i = 1,\ldots,t-1$ are rational functions in the variable z.

The necessary condition for the existence of bifurcations is that (6) has a unique solution, denoted as $\hat{\lambda}(e^{i\omega};\mu)$ for $z = e^{i\omega}$, crossing over the critical point $-1 + i0$ for $\mu = \mu_o$ and a frequency ω_o. In that way, saddle-node, transcritical or pitchfork bifurcations are characterized by $\omega_o = 0$, period-doubling bifurcations are defined by $\omega_o = \omega_D = \pi$ and Hopf bifurcations are restricted to a value of $\omega_o = \omega_H$ which excludes the points $e^{in\omega_H} = 1$ for $n = 1,2,3,4$.

An analogous treatment can be carried out to detect some of the degeneracies frequently exhibited by discrete-time systems but, in this case, using additional information of $g_0(\lambda;z;\mu)$ as well. For instance, taking into account that a double root in z of (6) is found via the expression

$$g_1(\lambda_o;z_o;\mu_o) = \left.\frac{\partial g_0(\lambda;z;\mu)}{\partial z}\right|_{\lambda=\lambda_o, z=z_o, \mu=\mu_o} = 0\,, \tag{7}$$

strong 1:1 resonance points can be distinguished by the conditions $\hat{\lambda}(1;\mu_o) = -1 + i0$ [or, equivalently, $g_0(-1;1;\mu_o) = 0$] and $g_1(-1;1;\mu_o) = 0$. Analogously, the appearance of strong 1:2 resonance points implies the verification of $\hat{\lambda}(e^{i\omega_D};\mu_o) = -1 + i0$ [or $g_0(-1;e^{i\omega_D};\mu_o) = 0$] and $g_1(-1;e^{i\omega_D};\mu_o) = 0$. The other two strong resonances can also be determined easily. In those cases, the unique restriction is that the eigenvalue $\hat{\lambda}(e^{i\omega};\mu)$ crosses the point $-1 + i0$ under the assumption $e^{in\omega_o} = 1$ with $n = 3,4$ for strong 1:3 or 1:4 resonance points, respectively. The interested reader should consult Peckham *et al.* [1995] for the subtleties of the interactions of resonance horns and Hopf bifurcations.

In the following, we will focus our attention on other common degeneracies which occur when the so-called stability indices of period-doubling and Hopf bifurcations vanish. This type of singularity is related to the appearance of multiple solutions in the continuation of period-two points or invariant orbits, respectively, after varying the main bifurcation parameter.

For simplicity, the failure of the transversality condition will not be considered here. Instead, it will be assumed that the eigenvalue passes over $-1 + i0$ with a definite sign of its derivative with respect to the bifurcation parameter. However, an inclusion of the transversality condition for maps could be possible, extending the results given in [Itovich & Moiola, 2002] for continuous-time feedback systems.

3. Approximation of Degenerate Bifurcations

Frequency-domain approaches to study nondegenerate Hopf and period-doubling bifurcations have already been presented in [D'Amico *et al.*, 2002, 2003a]. Based on the application of a second-order harmonic balance, these methods allow not only the

[1]For simplicity, the adopted notation is $D_i f(\hat{x};\mu) = \partial^i f(x;\mu)/\partial x^i|_{x=\hat{x}}$, even if $x \in \mathbf{R}^n$.

approximation of the emerging orbit but also the determination of its stability. However, they fail when the bifurcation degenerates due to the vanishing of their first stability indices. A natural solution of that inconvenience is the application of the following higher-order harmonic balance method.

In general, if μ is set nearly equal to μ_o, so that the eigenvalue $\hat{\lambda}(e^{i\omega};\mu)$ lies near $-1+i0$ at a frequency ω close to ω_o, an orbit emerging from the fixed point $\hat{y}$ can be approximated as

$$y_k = \hat{y} + \mathrm{Re}\left\{\sum_{r=0}^{2q} Y_r e^{ir\omega k}\right\} \tag{8}$$

where y_k, $\hat{y} \in \mathbf{R}^m$, $Y_r \in \mathbf{C}^m$, and "Re" stands for "real part". Based on the hypothesis that the nonlinear function $f(\cdot\,;\cdot)$ is at least C^{2q+1}, its expansion with respect to y_k in Taylor series up to the $(2q+1)$-order is given by

$$f(y_k;\mu) = f(\hat{y};\mu) + \sum_{j=1}^{2q+1} \frac{1}{j!} D_j f(\hat{y};\mu)(y_k-\hat{y})^j + O(|y_k-\hat{y}|^{2q+2})\,.$$

Thus, replacing y_k with (8), it is found that

$$f(y_k;\mu) = f(\hat{y};\mu) + \mathrm{Re}\left\{\sum_{r=0}^{2q} F_r e^{ir\omega k}\right\} + O(|y_k-\hat{y}|^{2q+2})\,, \tag{9}$$

where each F_r will depend on the coefficient vectors Y_r, the Jacobian $J(\mu)$ and the derivatives $D_j f(\hat{y};\mu)$, $j = 2,\ldots,2q+1$. Since the function $f(\cdot\,;\cdot)$ has the same frequency components as (8), the harmonic balance principle states that $Y_r = -G(e^{ir\omega};\mu)F_r$. Therefore, it is possible to solve for the vectors Y_r and so to approximate the actual solution. In Secs. 3.1 and 3.2, this procedure is used to analyze period-doubling and Hopf bifurcations, respectively.

3.1. *Period-doubling bifurcations*

In this case, the frequency ω of the periodic solutions equals $\omega_D = \pi$, and thus the approximation (8) considering period-two orbits can be simplified as

$$y_k^D = \hat{y} + Y_0^D + Y_1^D e^{i\omega_D k}, \tag{10}$$

where $\hat{y}$, Y_0^D, $Y_1^D \in \mathbf{R}^m$. Assuming that each Y_r^D depends polynomially on the amplitude θ of the orbit,

$$Y_r^D = \sum_{j=1}^{q+r} V_{r,2j-r}^D \theta^{2j-r}\,, \tag{11}$$

where $V_{r,2j-r}^D$ are real coefficient vectors to be determined through the harmonic balance, the expansion (9) can be written as

$$f(y_k^D;\mu) = f(\hat{y};\mu) + F_0^D + F_1^D e^{i\omega_D k} + O(\theta^{2q+2})$$

with

$$F_r^D = J(\mu)Y_r^D + \sum_{j=1}^{q} W_{r,2j+r}^D \theta^{2j+r} \tag{12}$$

and each $W_{r,2j+r}^D$ is a function of both the derivatives $D_j f(\hat{y};\mu)$ up to the $(2j+r)$-order and the vectors $V_{r,l}^D$ with $l < 2j+r$. The harmonic balance equations are $Y_r^D = -G(e^{ir\omega_D};\mu)F_r^D$. Then, substituting (11) and (12) in the corresponding Y_r^D and F_r^D, and rearranging terms, it yields

$$[I + G(e^{ir\omega_D};\mu)J(\mu)] \sum_{j=1}^{q+r} V_{r,2j-r}^D \theta^{2j-r} = -G(e^{ir\omega_D};\mu) \sum_{j=1}^{q} W_{r,2j+r}^D \theta^{2j+r} + O(\theta^{2q+2})\,. \tag{13}$$

The balance for the zero frequency can be computed setting $r = 0$, and thus (13) can be expressed as

$$[I + G(1;\mu)J(\mu)] \sum_{j=1}^{q} V_{0,2j}^D \theta^{2j} = -G(1;\mu) \sum_{j=1}^{q} W_{0,2j}^D \theta^{2j} + O(\theta^{2q+2})\,. \tag{14}$$

Since by hypothesis the eigenvalue of $G(e^{i\omega};\mu)J(\mu)$ passes over the point $-1+i0$ only for the frequency $\omega = \omega_D = \pi$, the matrix on the left-hand side is nonsingular. Then, Eq. (14) can be written in the explicit form

$$\sum_{j=1}^{q} V_{0,2j}^D \theta^{2j} = -H(1;\mu) \sum_{j=1}^{q} W_{0,2j}^D \theta^{2j} + O(\theta^{2q+2})\,,$$

where $H(1;\mu)$ is the closed-loop matrix[2] evaluated at $z = 1$. Equating the terms of equal powers in θ, it is found that $V_{0,2j}^D = -H(1;\mu)W_{0,2j}^D$. Therefore,

[2] $H(z;\mu) = [G(z;\mu)J(\mu) + I]^{-1}G(z;\mu)$.

each $V^D_{0,2j}$ can be calculated progressively once the coefficient vectors $V^D_{0,2j'}$ and $V^D_{1,2j'+1}$ with $j' < j$ are known.

The balance equation (13) at the frequency of a period-two solution ($r = 1$) is given by

$$[I + G(e^{i\omega_D};\mu)J(\mu)] \sum_{j=1}^{q+1} V^D_{1,2j-1}\theta^{2j-1} = -G(e^{i\omega_D};\mu) \sum_{j=1}^{q} W^D_{1,2j+1}\theta^{2j+1} + O(\theta^{2q+2}),$$

which can further be simplified to

$$[I + G(-1;\mu)J(\mu)] \sum_{j=0}^{q} V^D_{1,2j+1}\theta^{2j} = -G(-1;\mu) \sum_{j=1}^{q} W^D_{1,2j+1}\theta^{2j} + O(\theta^{2q+1}), \quad (15)$$

if $\theta \neq 0$. As mentioned before, the matrix $I + G(z;\mu)J(\mu)$ is singular for $z = -1$, and therefore, it is not possible to solve (15) to provide an explicit expression for each $V^D_{1,2j+1}$. However, this difficulty may be overcome as proposed in [Mees & Chua, 1979] and in [D'Amico *et al.*, 2003a] for the continuous- and discrete-time cases, respectively. Hence, it is assumed that V^D_{11} is the right eigenvector of $G(e^{i\omega_D};\mu)J(\mu)$ associated with $\hat{\lambda}(e^{i\omega_D};\mu)$ and that the vectors $V^D_{1,2j+1}$ (with $j = 1, 2, \ldots, q$) are correction terms of the main contribution $V^D_{11}\theta$ and they are orthogonal to V^D_{11}. Furthermore, each $V^D_{1,2j+1}$ can be obtained from

$$P_D[I + G(-1;\mu)J(\mu)]V^D_{1,2j+1} = -P_D G(-1;\mu)W^D_{1,2j+1}, \quad j = 1, 2, \ldots, q \quad (16)$$

where P_D is the projection matrix[3] on the subspace orthogonal to V^D_{11}.

Since the expressions necessary to compute all the coefficients $V^D_{r,2j-r}$ in (11) have already been derived, the amplitude θ of the period-two solution can be obtained as follows. Premultiplying both sides by s^T which is the left eigenvector of $G(e^{i\omega_D};\mu)J(\mu)$ associated with $\hat{\lambda}(e^{i\omega_D};\mu)$, (15) can be expressed as

$$[1 + \hat{\lambda}(-1;\mu)] \sum_{j=0}^{q} s^T V^D_{1,2j+1}\theta^{2j} = -s^T G(-1;\mu) \sum_{j=1}^{q} W^D_{1,2j+1}\theta^{2j} + O(\theta^{2q+1}). \quad (17)$$

Assuming that the eigenvalue $\hat{\lambda}(e^{i\omega};\mu)$ calculated at $\omega = \omega_D = \pi$ is given by

$$\hat{\lambda}(-1;\mu) = -1 + \sum_{m=1}^{q} \xi^D_m(\mu)\theta^{2m} + O(\theta^{2q+2}) \quad (18)$$

with $\xi_m(\mu) \in \mathbf{R}$, after some routine calculations (17) can be rewritten as

$$\sum_{j=1}^{q} \xi^D_j(\mu) s^T V^D_{11}\theta^{2j} = -\sum_{j=1}^{q} \left[s^T G(-1;\mu) W^D_{1,2j+1}\theta^{2j} + \sum_{m=1}^{q-j} \xi^D_m(\mu) s^T V^D_{1,2j+1}\theta^{2(m+j)} \right] + O(\theta^{2q+1}).$$

Grouping together terms of equal power in θ,

$$\xi^D_j(\mu) = -\frac{1}{s^T V^D_{11}} \left[s^T G(-1;\mu) W^D_{1,2j+1} + \sum_{m=1}^{j-1} \xi^D_{j-i}(\mu) s^T V^D_{1,2m+1} \right].$$

Once each of these coefficients $\xi^D_j(\mu)$ has been calculated, (18) can be used to detect a possible intersection between the Nyquist locus of $\hat{\lambda}(e^{i\omega};\mu)$ and a curve parameterized by θ. If an intersection occurs at the point $q_{PD} = \hat{\lambda}(-1;\mu_{PD})$, the solution θ_{PD} provides an estimation of the amplitude of the approximate period-two orbit (10) for the parameter value μ_{PD}.

3.2. *Hopf bifurcations*

This section summarizes the main results given in [D'Amico *et al.*, 2003b] for the study of Hopf bifurcations via a higher-order harmonic balance. The

[3]The projection matrix on a subspace orthogonal to a vector X is given by $P = I - (X^T X)^{-1} X X^T$ with "$(\cdot)^T$" representing the transpose conjugate operator.

approximate solution is given by (8) where the coefficient vector Y_r^H associated with the rth harmonic is defined as

$$Y_r^H = \sum_j V_{rj}^H \theta^j \tag{19}$$

with $V_{rj}^H \in \mathbf{C}^m$ and j varying from r (or 2 for $r = 0$) in steps of 2 up to the order $2q+1$ (or $2q$ for r even). Thus, each F_r^H can be written as

$$F_r^H = J(\mu) Y_r^H + \sum_j W_{rj}^H \theta^j \,, \tag{20}$$

where the index j takes the same values as before and the vectors W_{rj}^H are functions of higher-order derivatives of $f(\cdot;\cdot)$ and the $V_{r'j'}^H$ with $r' \le r$ and $r' + j' \le r + j$, except for the $r = 0$ case.

Replacing (19) and (20) in the balance equations, the relationship among the vectors is obtained as

$$\begin{aligned}[I + G(e^{ir\omega};\mu)J(\mu)]V_{rj}^H \\ = -G(e^{ir\omega};\mu)W_{rj}^H \,.\end{aligned} \tag{21}$$

Since matrix $I + G(e^{ir\omega};\mu)J(\mu)$ is nonsingular for $r \neq 1$, (21) can be rewritten as $V_{rj}^H = -H(e^{ir\omega};\mu)W_{rj}^H$ and then V_{rj}^H, with $r \neq 1$, can be computed taking into account that the vectors $V_{1j'}^H$ with $j' \le j$ are known. However, for $r = 1$, this matrix is singular at the criticality and, as in the case of period-doubling bifurcations, (21) cannot be solved explicitly for V_{1j}^H. Again, it is assumed that V_{11}^H is the right eigenvector of $G(e^{i\omega};\mu)J(\mu)$ associated with the eigenvalue $\hat{\lambda}(e^{i\omega};\mu)$, and V_{1j}^H with $j = 3, 5, \ldots, q$ are orthogonal to V_{11}^H. Hence, each vector V_{1j}^H is computed from

$$\begin{aligned}P_H[I + G(e^{i\omega};\mu)J(\mu)]V_{1,2j+1}^H \\ = -P_H G(e^{i\omega};\mu)W_{1,2j+1}^H \,,\end{aligned}$$

where $j = 1, 2, \ldots, q$ and P_H is the projection matrix defined before but in this case for Hopf bifurcations.

Now, the harmonic balance equation for $r = 1$ is

$$\begin{aligned}[I + G(e^{i\omega};\mu)J(\mu)] \sum_{j=0}^{q} V_{1,2j+1}^H \theta^{2j} \\ = -G(e^{i\omega};\mu) \sum_{j=1}^{q} W_{1,2j+1}^H \theta^{2j} \\ + O(\theta^{2q+1}) \,.\end{aligned} \tag{22}$$

Premultiplying both sides by s^T, which is the left eigenvector of $G(e^{i\omega};\mu)J(\mu)$ associated with $\hat{\lambda}(e^{i\omega};\mu)$, and considering

$$\hat{\lambda}(e^{i\omega};\mu) = -1 + \sum_{m=1}^{q} \xi_m^H(\mu)\theta^{2m} + O(\theta^{2q+2}) \,, \tag{23}$$

Eq. (22) can be expressed as

$$\begin{aligned}\sum_{m=1}^{q} \xi_m^H(\mu)\theta^{2m} \sum_{j=0}^{q} s^T V_{1,2j+1}^H \theta^{2j+1} \\ = -s^T G(e^{i\omega};\mu) \sum_{j=1}^{q} W_{1,2j+1}^H \theta^{2j+1} + O(\theta^{2q+1})\end{aligned}$$

and thus, each $\xi_j^H(\mu)$ is given by

$$\begin{aligned}\xi_j^H(\mu) = -\frac{1}{s^T V_{11}^H} \Bigg[s^T G(e^{i\omega};\mu) W_{1,2j+1}^H \\ + \sum_{m=1}^{j-1} \xi_{j-i}^H(\mu) s^T V_{1,2m+1}^H \Bigg] .\end{aligned}$$

Therefore, a similar geometrical interpretation as that described for period-two solutions can be applied. In fact, if the intersection occurs at a point $q_{HB} = \hat{\lambda}(e^{i\omega_{RH}};\mu_{HB})$, then not only the amplitude θ_{HB} but also the frequency ω_{HB} of the periodic solution can be obtained.

3.3. *Stability analysis*

To complete the frequency-domain study, the stability of the estimated orbits is analyzed by means of the so-called *stability indices*. Without loss of generality, let us consider that the fixed point $\hat{y}$ is stable for parameter values smaller than μ_o and that $\hat{\lambda}(z;\mu)$ crosses $-1 + i0$ modifying its stability as μ is increased. Moreover, let us suppose that the previous techniques ensure the existence of an orbit with small amplitude θ. Under these assumptions, the actual value of z for μ larger than μ_o can be defined as $\hat{z} = \rho e^{i\hat{\omega}}$, with $\rho > 1$ (see [D'Amico *et al.*, 2003b] for a more detailed definition). Then, the Taylor expansions around $\hat{z}$ of the different terms depending on z are given by

$$\begin{aligned}G(e^{i\omega};\mu) = G(\hat{z};\mu) \\ + \sum_{m=1}^{q} \frac{1}{m!} (e^{i\omega} - \hat{z})^m D_m G(\hat{z};\mu) \,,\end{aligned} \tag{24}$$

$$V_{11} = \hat{V}_{11} + \sum_{m=1}^{q} \frac{1}{m!} (e^{i\omega} - \hat{z})^m D_m V_{11} \,, \tag{25}$$

$$V_{1,2j+1} = \hat{V}_{1,2j+1} + \sum_{m=1}^{q} \frac{1}{m!} (e^{i\omega} - \hat{z})^m D_m V_{1,2j+1}\,, \quad (26)$$

$$W_{1,2j+1} = \hat{W}_{1,2j+1} + \sum_{m=1}^{q} \frac{1}{m!} (e^{i\omega} - \hat{z})^m D_m W_{1,2j+1}\,, \quad (27)$$

where $j = 1, 2, \ldots, q$, V_{11}, $V_{1,2j+1}$ and $W_{1,2j+1}$ can be any of the coefficient vectors corresponding to period-doubling or Hopf bifurcations and $\hat{V}_{11}$, $\hat{V}_{1,2j+1}$, $\hat{W}_{1,2j+1}$ are the vectors V_{11}, $V_{1,2j+1}$, $W_{1,2j+1}$ evaluated at $\hat{z}$, respectively. For clarity, the arguments in V_{11}, $V_{1,2j+1}$, $W_{1,2j+1}$ as well as in their derivatives have been omitted. The expansion of the eigenvector V_{11} is taken into account in order to build up more accurate results comparing with those obtained in [Moiola & Chen, 1996].

In addition, the balance equations (15) of period-doubling bifurcations and (22) of Hopf bifurcations can be unified as

$$[I + G(e^{i\tilde{\omega}}; \mu) J(\mu)] \sum_{j=0}^{q} V_{1,2j+1} \theta^{2j} = -G(e^{i\tilde{\omega}}; \mu) \sum_{j=1}^{q} W_{1,2j+1} \theta^{2j} + O(\theta^{2q+1})\,. \quad (28)$$

Notice that $\tilde{\omega} = \omega_D$ for period-two orbits or $\tilde{\omega} = \omega$ close to ω_H for invariant orbits emerging from Hopf bifurcations. Substituting (24)–(27) into (28) and premultiplying both sides by s^T,

$$s^T \left[\sum_{m=1}^{q} \frac{(e^{i\tilde{\omega}} - \hat{z})^m}{m!} D_m G(\hat{z}; \mu) \right] J(\mu) \sum_{j=0}^{q} \left[\hat{V}_{1,2j+1} + \sum_{m=1}^{q} \frac{(e^{i\tilde{\omega}} - \hat{z})^m}{m!} D_m V_{1,2j+1} \right] \theta^{2j} = -s^T \left[\sum_{m=0}^{q} \frac{(e^{i\tilde{\omega}} - \hat{z})^m}{m!} D_m G(\hat{z}; \mu) \right] \sum_{j=1}^{q} \left[\hat{W}_{1,2j+1} + \sum_{m=1}^{q} \frac{(e^{i\tilde{\omega}} - \hat{z})^m}{m!} D_m W_{1,2j+1} \right] \theta^{2j} + O(\theta^{2q+1})\,. \quad (29)$$

Several higher-order approximations of (29) will be used to define the different stability indices. The first one is obtained considering that the term $(e^{i\tilde{\omega}} - \hat{z})$ is $O(\theta^2)$. In that case, (29) can be simplified as

$$(e^{i\tilde{\omega}} - \hat{z}) s^T D_1 G(\hat{z}; \mu) J(\mu) V_{11} = -s^T G(\hat{z}; \mu) \hat{W}_{13} \theta^2 + O(\theta^4)\,,$$

which is equivalent to

$$(e^{i\tilde{\omega}} - \hat{z}) = \gamma_1 \theta^2 + O(\theta^4) \quad (30)$$

where

$$\gamma_1 \doteq -\frac{s^T G(\hat{z}; \mu) \hat{W}_{13}}{s^T D_1 G(\hat{z}; \mu) J(\mu) V_{11}}\,.$$

Substituting (30) into (29), assuming that $(e^{i\tilde{\omega}} - \hat{z})$ is $O(\theta^4)$ and grouping together coefficients of equal power in θ, the new approximation can be defined in the compact form

$$(e^{i\tilde{\omega}} - \hat{z}) = \gamma_1 \theta^2 + \gamma_2 \theta^4 + O(\theta^6)\,, \quad (31)$$

where

$$\gamma_2 \doteq -\frac{1}{\eta} s^T \Big\{ \gamma_1 D_1 G(\hat{z}; \mu) [\hat{W}_{13} + J(\mu)(\hat{V}_{13} - \gamma_1 D_1 V_{11})] + \gamma_1 G(\hat{z}; \mu) D_1 \hat{W}_{13} - \frac{1}{2} \gamma_1^2 D_2 G(\hat{z}; \mu) J(\mu) V_{11} + G(\hat{z}; \mu) \hat{W}_{15} \Big\}$$

with $\eta = s^T D_1 G(\hat{z}; \mu) J(\mu) V_{11}$. Following a similar reasoning, now substituting (31) into (29), it is possible to arrive at the next higher-order approximation. The same steps can be repeated until the desired order of accuracy is obtained.

In principle, the first approximation of (29) allows us to determine the stability of the emerging orbits. Assuming that $\delta\omega = \tilde{\omega} - \hat{\omega}$, (30) can also be expressed as

$$e^{i\delta\omega} - \rho = \gamma_1 e^{-i\hat{\omega}} \theta^2 + O(\theta^4)\,,$$

and then, considering the real part,

$$\rho - \mathrm{Re}\{e^{i\delta\omega}\} = \mathrm{Re}\{-\gamma_1 e^{-i\hat{\omega}}\} \theta^2 + O(\theta^4)\,. \quad (32)$$

Taking into account that $\rho > 1$, the left-hand side of this equation is always greater than zero. Therefore, to have a supercritical bifurcation, i.e. a stable solution $\theta^2 > 0$ for $\mu > \mu_o$, it is necessary that

$$\sigma_1 = \mathrm{Re}\left\{ \frac{s^T G(e^{i\hat{\omega}};\mu)\hat{W}_{13} e^{-i\hat{\omega}}}{s^T D_1 G(e^{i\hat{\omega}};\mu) J(\mu) V_{11}} \right\} > 0\,.$$

Analogously, it can be derived that a subcritical bifurcation occurs when $\sigma_1 < 0$. In the following, we will refer to σ_1 as the *first stability index.*

Now, when the first stability index vanishes, the bifurcation degenerates and the local behavior becomes more complex. In that case, the stability of the emerging orbits may be determined taking into account the real part of the fourth-order expansion (31), i.e.

$$\rho - \mathrm{Re}\{e^{i\delta\omega}\} = \mathrm{Re}\{-\gamma_1 e^{-i\hat{\omega}}\}\theta^2 + \mathrm{Re}\{-\gamma_2 e^{-i\hat{\omega}}\}\theta^4 + O(\theta^6)\,,$$

and defining the second stability index $\sigma_2 = \mathrm{Re}\{\gamma_2 e^{-i\hat{\omega}}\}$. Thus, there will exist a stable solution at the degenerate point ($\sigma_1 = 0$) for $\sigma_2 > 0$ or an unstable one for $\sigma_2 < 0$. In a neighborhood of the degeneracy the sign of both indices should be analyzed to establish the dynamics of the system. In fact, a unique solution is ensured only if the indices have the same sign while multiple solutions can be expected in the case of opposite signs. Finally, if both σ_1 and σ_2 vanish at the same point for certain critical combination of the parameters, it is necessary to study the sign of the third stability index corresponding to the term θ^6, and so on.

Notice that the stability indices depend on the frequency of the exact solution. However, for Hopf bifurcations, a classification of the singularity can also be obtained computing them at ω_H, i.e. the frequency at which the Nyquist diagram of $\hat{\lambda}(e^{i\omega};\mu_o)$ passes over the critical point $-1 + i0$. In a similar way, since for period-doubling bifurcations $\hat{\omega} = \omega_D = \pi$, the expressions of the stability indices are simpler to compute. Hence, index σ_1 is given by

$$\sigma_{1PD} = -\frac{s^T G(-1;\mu) W_{13}^D}{s^T D_1 G(-1;\mu) J(\mu) V_{11}^D} \tag{33}$$

and σ_2 can be obtained as

$$\begin{aligned}\sigma_{2PD} = -\frac{1}{\eta}\, s^T \Big\{ & \sigma_{1PD} D_1 G(-1;\mu)[W_{13}^D + J(\mu) V_{13}^D] \\ & + \sigma_{1PD} G(-1;\mu) D_1 W_{13}^D \\ & + \frac{1}{2}\sigma_{1PD}{}^2 D_2 G(-1;\mu) J(\mu) V_{11}^D \\ & + G(-1;\mu) W_{15}^D \Big\}. \end{aligned} \tag{34}$$

4. Examples

In this section, the dynamical behavior of two discrete-time systems is analyzed using the methodology developed above. The first example shows the approximation of the degenerate period-doubling bifurcations in an adaptive control system. Furthermore, the results are compared with those obtained by the continuation package AUTO. The second example gives a general description of the different degenerate bifurcations presented in the controlled Hénon map.

4.1. *A simple adaptive control system*

Let us consider the adaptive control system proposed in [Golden & Ydstie, 1988] consisting of a first-order plant with an uncertain pole α and an unknown (but fixed) gain. The map including the plant, the controller and the estimator is

$$x_{k+1}^1 = -\alpha x_k^1 + \beta(\hat{x} - x_k^2 x_k^1)\,,$$

$$x_{k+1}^2 = x_k^2 + \frac{p x_k^1}{c + (x_k^1)^2}\left[-\alpha x_k^1 + \beta(\hat{x} - x_k^2 x_k^1) - \hat{x}\right],$$

where x_k^1 is the state variable of the plant, x_k^2 is the estimation of α, β is a factor that represents the quotient between the actual gain of the plant and its supposed value, $\hat{x}$ is the expected value of x_k^1, p is the gain of the estimation algorithm and c is a parameter which avoids the division by zero. However, it will be shown that this last parameter is also of importance for determing the dynamical behavior of the system.

The adoption of the matrices

$$A = \begin{bmatrix} -\alpha & 0 \\ 0 & 1 \end{bmatrix}, \quad B = C = \begin{bmatrix} 1 & 0 \\ 0 & 1 \end{bmatrix},$$

$$D = \begin{bmatrix} d_1 & 0 \\ 0 & d_2 \end{bmatrix},$$

and the function

$$h(\cdot;\cdot) = \begin{bmatrix} \beta(\hat{x} - x_k^2 x_k^1) \\ \dfrac{p x_k^1}{c + (x_k^1)^2}\left[-\alpha x_k^1 + \beta(\hat{x} - x_k^2 x_k^1) - \hat{x}\right] \end{bmatrix},$$

with the constants $d_1 = 2 + \alpha - \beta$ and $d_2 = -p\hat{x}\beta(2 - \beta)/(c + \hat{x}^2)$, allows us to transform the adaptive system into the equivalent feedback

representation

$$G(z;\mu)=\begin{bmatrix}\dfrac{1}{z+\alpha-d_1} & 0\\ 0 & \dfrac{1}{z-(1+d_2)}\end{bmatrix},$$

$$f(y_k;\mu)=\begin{bmatrix} d_1 y_k^1-\beta(\hat{x}-y_k^2 y_k^1)\\ d_2 y_k^2+\dfrac{p y_k^1}{c+(y_k^1)^2}\left[\alpha y_k^1-\beta(\hat{x}-y_k^2 y_k^1)+\hat{x}\right]\end{bmatrix},$$

defining $y_k=[y_k^1 \quad y_k^2]^T$ as the output of the closed-loop and $\mu=(\alpha,\beta,c,p)$ as the parameter vector. The values of d_1 and d_2, otherwise arbitrary, have been chosen so that the matrix $G(z;\mu)J(\mu)$ has a single relevant eigenvalue.

The fixed point is obtained by solving (5), yielding $\hat{y}=[\hat{x} \quad -(1+\alpha-\beta)/\beta]^T$. Moreover, the linearization of $f(y_k;\mu)$ around this fixed point is given by

$$J(\mu)=\begin{bmatrix} d_1+\beta-(1+\alpha) & \beta\hat{x}\\ -\dfrac{p\hat{x}(1-\beta)}{c+\hat{x}^2} & d_2+\dfrac{p\hat{x}^2\beta}{c+\hat{x}^2}\end{bmatrix},$$

and so the unique nontrivial eigenvalue of $G(e^{i\omega};\mu)J(\mu)$ is

$$\hat{\lambda}(e^{i\omega};\mu)=\frac{1}{z-(2-\beta)} - \frac{\beta p\hat{x}^2(1-\beta)}{(c+\hat{x}^2)z-[c+\hat{x}^2(1-2\beta p+\beta^2 p)]}.$$

The crossing condition $\hat{\lambda}(e^{i\omega_o};\mu_o)=-1+i0$ is verified only if $\omega_o=\omega_D$ and this occurs when the parameter β satisfies

$$\beta_o=\frac{4(c+\hat{x}^2)}{\hat{x}^2 p+2(c+\hat{x}^2)}. \tag{35}$$

In that case, an approximation of the orbit emerging from a period-doubling bifurcation can be computed following the procedure presented before. Without loss of generality, it is assumed that $p=1$.

The right and left eigenvectors associated with $\hat{\lambda}(e^{i\omega};\mu)$ are

$$V_{11}^D=\begin{bmatrix}v_1\\1\end{bmatrix}=\begin{bmatrix}-\dfrac{2c+\hat{x}[1+(1-\beta)^2]}{(3-\beta)(1-\beta)\hat{x}}\\ 1\end{bmatrix},$$

$$s^T=[1 \quad \beta\hat{x}].$$

Taking into account the formulas corresponding to a second-order approximation (see Appendix), the other vectors are given by

$$V_{02}^D=\frac{v_1(c-\hat{x}^2)}{\hat{x}^2(c+\hat{x}^2)}\begin{bmatrix}[\beta\hat{x}-(1-\beta)v_1]\hat{x}\\ (1-\beta)v_1-\beta\hat{x}-\hat{x}\dfrac{c+\hat{x}^2}{c-\hat{x}^2}\end{bmatrix}$$

and $W_{13}^D=[w_{13a} \quad w_{13b}]^T$ with

$$w_{13a}=-\frac{v_1\beta(c-\hat{x}^2)(\hat{x}-v_1)}{\hat{x}^2(c+\hat{x}^2)}[(1-\beta)v_1 - \beta\hat{x}]-\frac{\beta v_1^2}{\hat{x}},$$

$$w_{13b}=\frac{1}{\hat{x}(c+\hat{x}^2)^3}\{2v_1^2[(1-\beta)v_1 - \beta\hat{x}][(1-\beta)(c-\hat{x}^2)^2+\hat{x}^2 c] - v_1(c-\hat{x}^2)[c(2w_{13a}-v_1\beta\hat{x}) - v_1^2\hat{x}^2(1-\beta)]\}.$$

Therefore,

$$\xi_1^D(\mu)=-\frac{(c-\hat{x}^2)[v_1 w_{13a}(1-\beta)-\beta w_{13b}(c+\hat{x}^2)]}{\hat{x}^2(c+\hat{x}^2)(v_1+\beta\hat{x})(3-\beta)(1-\beta)}.$$

Once the Nyquist diagram of $\hat{\lambda}(e^{i\omega};\mu)$ intersects the half-line starting at $-1+i0$ in the direction of $\xi_1^D(\mu)$, the stability of the emerging period-two orbit is determined calculating (33) at the criticality. Thus, the first stability index is found to be

$$\sigma_{1PD}=\frac{2(31\beta^3-144\beta^2+232\beta-128)}{\beta(2-\beta)^2}. \tag{36}$$

As can be observed, the sign of (36) depends on the values of parameter β. In fact, index σ_{1PD} assures the existence of a supercritical bifurcation if $\beta>\beta_o=1.43537$ and a subcritical one if $\beta<\beta_o$. For $\beta=\beta_o$, index σ_{1PD} vanishes so that the adaptive system exhibits a degenerate period-doubling bifurcation. Then, the second-order approximation fails and the computation of the next higher-order balance is required in order to characterize the orbit emerging from that point.

Due to the extension of the expressions, only the stability analysis of the fourth-order approximation is shown. In that way, if the locus of $\hat{\lambda}(e^{i\omega};\mu)$ intersects the curve $-1+\xi_1^D(\mu)\theta^2+\xi_2^D(\mu)\theta^4$ for some combination of the parameters, the first stability index is given by (36), and the second one, calculated at the degeneracy, is obtained as

$$\sigma_{2PDO}=\frac{44.6111\hat{x}^2+6.8933}{\hat{x}^2+0.1547}.$$

Therefore, considering that there exists a neighborhood of the degenerate point in which $\sigma_{2PD}>0$,

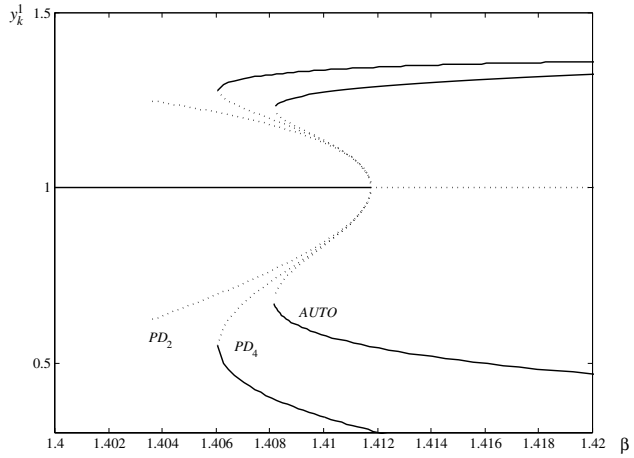

Fig. 2. Local bifurcation diagram of the adaptive control system for $\alpha = 1$, $\hat{x} = 1$, $p = 1$ and $c = 0.2$. (−) stable solution; (−−) unstable solution; $AUTO$: exact period-two orbit; PD_2: second-order approximation; PD_4: fourth-order approximation.

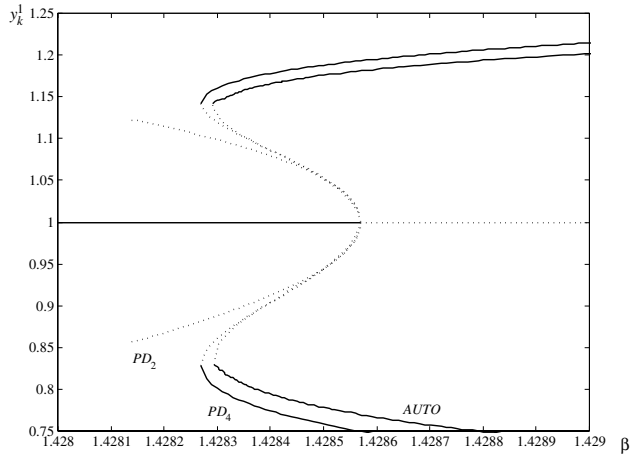

Fig. 3. Local bifurcation diagram of the adaptive control system for $\alpha = 1$, $\hat{x} = 1$, $p = 1$ and $c = 0.25$. (−) stable solution; (−−) unstable solution; $AUTO$: exact period-two orbit; PD_2: second-order approximation; PD_4: fourth-order approximation.

it can be seen that the supercritical bifurcation remains as a single solution when $\beta \geq \beta_o$ ($\sigma_{1PD} > 0$, $\sigma_{2PD} > 0$). For $\beta < \beta_o$, the alternation in sign ($\sigma_{1PD} < 0$, $\sigma_{2PD} > 0$) enables the presence of multiple solutions. Thus, the predicted unstable period-two points coexist with a stable period-two orbit.

Figures 2 to 5 show the projections on the (y_k^1, β)-plane of the degenerate period-doubling bifurcations obtained by both the second- and the fourth-order approximation compared to those calculated by using AUTO for $\alpha = 1$, $\hat{x} = 1$ and different values of parameter c. As can be seen in

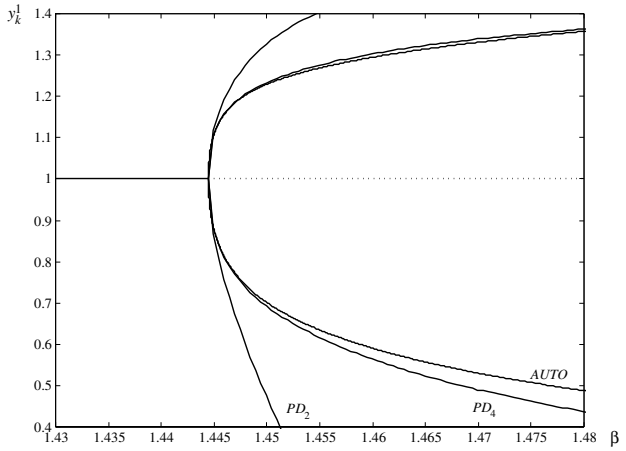

Fig. 4. Local bifurcation diagram of the adaptive control system for $\alpha = 1$, $\hat{x} = 1$, $p = 1$ and $c = 0.3$: (−) stable solution; (−−) unstable solution; $AUTO$: exact period-two orbit; PD_2: second-order approximation; PD_4: fourth-order approximation.

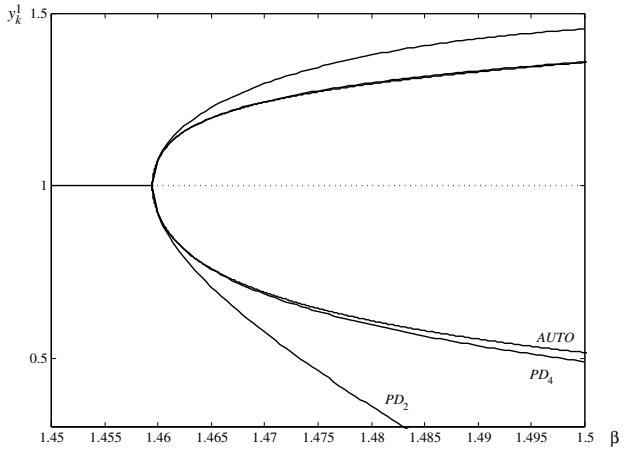

Fig. 5. Local bifurcation diagram of the adaptive control system for $\alpha = 1$, $\hat{x} = 1$, $p = 1$ and $c = 0.35$: (−) stable solution; (−−) unstable solution; $AUTO$: exact period-two orbit; PD_2: second-order approximation; PD_4: fourth-order approximation.

Figs. 2 and 3, the second-order approximation fails to detect the saddle-node bifurcation of the period-two branch. On the other hand, the fourth-order approximation gives an acceptable estimation of the saddle-node location compared to AUTO and recovers the coexisting multiplicity of solutions. In brief, all the figures reveal that the fourth-order solution predicts more acceptably the unfoldings of the degeneracy.

4.2. *The controlled Hénon map*

The discrete-time model consisting of the Hénon map together with a washout filter and a nonlinear

control law is given by

$$\begin{aligned} x_{k+1}^1 &= \rho + p x_k^2 - (x_k^1)^2 + \tilde{u}_k \,, \\ x_{k+1}^2 &= x_k^1 \,, \\ w_{k+1} &= x_k^1 + (1-d) w_k \,, \\ z_k &= x_k^1 - d w_k \,, \\ \tilde{u}_k &= k_1 z_k + k_2 z_k^3 \,, \end{aligned}$$

where x_k^1, x_k^2, $\tilde{u}_k$ are the state variables and the control input of the map, w_k, z_k are the state variable and the output of the washout filter, respectively, ρ and p are parameters, k_1 and k_2 are control gains and d $(0 < d < 2)$ is a design coefficient. The Hénon map has been studied before by Abed *et al.* [1994] and Wen *et al.* [2002] using a washout filter controller (three-dimensional map), and by Shilnikov *et al.* [2001] without considering control (two-dimensional map). Moreover, a detailed frequency-domain analysis about the influences of k_1 and k_2 on the dynamics of the Hénon map has been presented in [D'Amico *et al.*, 2003a]. Here, we will concentrate on the appearance of different degenerate points as well as the complex phenomena around them due to the action of this nonlinear control law.

The previous model can be recast as a linear dynamical system — memoryless nonlinearity feedback connection by choosing the matrices

$$A = \begin{bmatrix} 0 & p & 0 \\ 1 & 0 & 0 \\ 1 & 0 & 1-d \end{bmatrix}, \quad B = \begin{bmatrix} 1 \\ 0 \\ 0 \end{bmatrix},$$

$$C = \begin{bmatrix} 1 & 0 & 0 \\ 1 & 0 & -d \end{bmatrix}, \quad D = \begin{bmatrix} 1 & 0 \\ 0 & 0 \end{bmatrix},$$

and the function

$$h(\cdot\,;\cdot) = \rho - (x_k^1)^2 + k_1 (x_k^1 - d w_k) + k_2 (x_k^1 - d w_k)^3 \,.$$

Then, the equivalent linear and nonlinear blocks (3) and (4) are given by

$$G(z;\mu) = \frac{z}{z^2 - z - p} \begin{bmatrix} 1 \\ \dfrac{z-1}{z-(1-d)} \end{bmatrix},$$

$$f(y_k;\mu) = -\rho + y_k^1 + (y_k^1)^2 - k_1 y_k^2 - k_2 (y_k^2)^3 \,,$$

respectively, $y_k = [x_k^1 \;\; x_k^1 - d w_k]^T$ being the output of the closed-loop and $\mu = (\rho, p, k_1, k_2)$ the parameter vector.

In this example, the fixed points are

$$\hat{y} = \begin{bmatrix} \hat{y}_\pm^1 \\ \hat{y}^2 \end{bmatrix} = \begin{bmatrix} \dfrac{1}{2}(p - 1 \pm \sqrt{(p-1)^2 + 4\rho}) \\ 0 \end{bmatrix},$$

and the linearization of $f(y_k;\mu)$ around them results in $J(\mu) = [1 + 2\hat{y}_\pm^1 \quad -k_1]$. Therefore, the algebraic equation (6) is given by

$$\begin{aligned} g_0(\lambda; z; \mu) = \lambda^2 &- \frac{z}{z^2 - z - p} \\ &\times \left[1 + 2\hat{y}_\pm^1 - k_1 \frac{z-1}{z-(1-d)} \right] \lambda = 0 \end{aligned}$$

with a single nontrivial solution

$$\begin{aligned} \hat{\lambda}(e^{i\omega}; \mu) = &\frac{e^{i\omega}}{e^{i2\omega} - e^{i\omega} - p} \\ &\times \left[1 + 2\hat{y}_\pm^1 - k_1 \frac{e^{i\omega} - 1}{e^{i\omega} - (1-d)} \right]. \end{aligned}$$

Depending on the values of the parameters, this system can develop different nondegenerated bifurcations. In fact, a saddle-node bifurcation ($\omega_o = 0$) occurs when ρ and p are related by

$$\rho_{SN} = -\frac{(1-p)^2}{4} \,. \tag{37}$$

For period-doubling bifurcations ($\omega_o = \omega_D$), the critical relationship among the parameters is

$$\begin{aligned} \rho_{PD} = &\frac{3}{4}(1-p)^2 + \frac{2(1-p)}{2-d} k_1 \\ &+ \frac{1}{(2-d)^2} k_1^2 \,. \end{aligned} \tag{38}$$

Finally, for Hopf bifurcations, the necessary condition is

$$\begin{aligned} \rho_{HB} = &\frac{1}{4(1-d)^2} \left[p(1-d)^2 + k_1 - 1 - \frac{p d k_1}{(1+p)^2} \right] \\ &\times \left[1 - p + k_1 - 2d + p d^2 - \frac{p d k_1}{(1+p)^2} \right] \end{aligned} \tag{39}$$

with $-1 + k_1/d < p < -1 + d k_1/(2-d)^2$.

A similar reasoning can be followed to find degenerate points lying on the (ρ, p)-plane. The computation of (7) results in

$$g_1(-1; e^{i\omega_o}; \mu_o) = \frac{1}{(e^{i2\omega_o} - e^{i\omega_o} - p)} \left[\frac{e^{i2\omega_o} + p}{e^{i\omega_o}} - \frac{k_1 d e^{i\omega_o}}{(e^{i\omega_o} - 1 + d)^2} \right] = 0 \,.$$

Table 1. Strong resonance points in the controlled Hénon map.

Resonance	Critical Condition	Parameter Value
1:1	$\rho = -\dfrac{(1-p)^2}{4}$	$p = -1 + \dfrac{k_1}{d}$
1:2	$\rho = \dfrac{3}{4}(1-p)^2 + \dfrac{2(1-p)}{2-d}\,k_1 + \dfrac{1}{(2-d)^2}\,k_1^2$	$p = -1 + \dfrac{dk_1}{(2-d)^2}$
1:3	$\rho = \dfrac{1}{4(1-d)^2}\left[-1 + p(1-d)^2 + \dfrac{1+p(1-d)}{1+p}k_1\right] \times \left[1 - 2d + p(1-d^2) + \dfrac{1+p(1-d)}{1+p}k_1\right]$	$p = -1 + \dfrac{dk_1}{3 - 3d + d^2}$
1:4	$\rho = \dfrac{1}{4(1-d)^2}\left[-1 + p(1-d)^2 + \dfrac{1+p(1-d)}{1+p}\,k_1\right] \times \left[1 - 2d + p(1-d^2) + \dfrac{1+p(1-d)}{1+p}\,k_1\right]$	$p = -1 + \dfrac{dk_1}{2 - 2d + d^2}$

Table 2. Vectors and coefficients for computing the fourth-order approximation of the period-two orbits in the controlled Hénon map.

$V_{02}^D = \left[\dfrac{-1}{1-p+2\hat{y}_\pm^1} \quad 0\right]^T$	$V_{04}^D = \left[\dfrac{-1}{(1-p+2\hat{y}_\pm^1)^3} \quad 0\right]^T$
$V_{11}^D = \left[1 \quad \dfrac{2}{2-d}\right]^T$	$V_{13}^D = \left[0 \quad 0\right]^T$
$W_{13}^D = -\dfrac{2}{1-p+2\hat{y}_\pm^1} - \dfrac{8k_2}{(2-d)^3}$	$W_{15}^D = -\dfrac{4}{(1-p+2\hat{y}_\pm^1)^3}$
$\xi_1^D(\mu) = \dfrac{W_{13}^D}{2-p}$	$\xi_2^D(\mu) = \dfrac{W_{15}^D}{2-p}$

Therefore, for the case $\omega_o = 0$, there will exist a strong 1:1 resonance if the parameters verify (37) when $p = -1 + k_1/d$. Analogously for $\omega_o = \omega_D = \pi$, a strong 1:2 resonance point is obtained when ρ is equal to (38) with $p = -1 + dk_1/(2-d)^2$. For the remaining strong resonance points, the condition (39) is verified for $\omega_o = 2\pi/3$ (1:3 resonance) when $p = -1 + dk_1/[3-(3-d)d]$ and for $\omega_o = \pi/2$ (1:4 resonance) when $p = -1 + dk_1/[2-(2-d)d]$. These conditions are summarized in Table 1 for the sake of clarity.

Whenever (38) or (39) are satisfied, an approximation of the orbit emerging from a period-doubling or Hopf bifurcation may easily be computed considering a second-order harmonic balance. However, if the stability condition fails, the dynamics around this degeneracy should be analyzed using higher-order terms. As before, the fourth-order harmonic balance method is considered to study the existence of degenerate period-two solutions. The corresponding vectors, computed using the formulas given in the Appendix, are depicted in Table 2. Then, assuming that the diagram of $\hat{\lambda}(e^{i\omega};\mu)$ intersects the curve $-1 + \xi_1^D(\mu)\theta^2 + \xi_2^D(\mu)\theta^4$ for some values of the parameter vector μ, the stability of the emerging period-two orbit could be determined

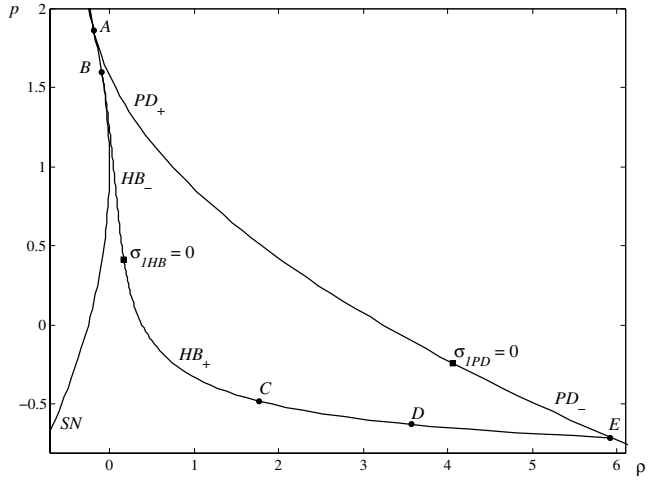

Fig. 6. Parameter plane of the controlled Hénon map ($k_1 = 1.3$, $k_2 = -0.2$).

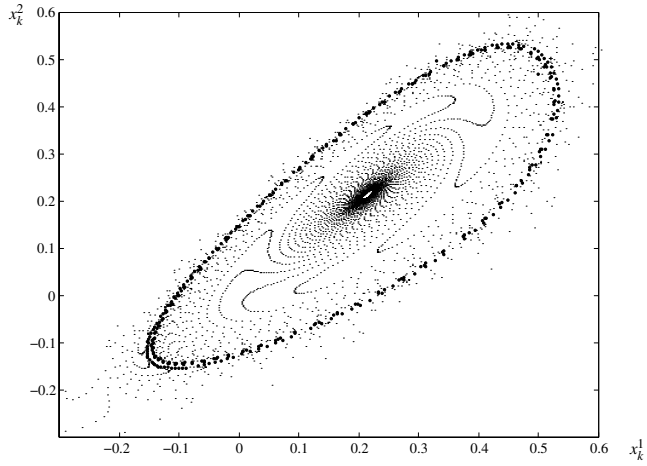

Fig. 7. Unstable invariant orbit of the controlled Hénon map for $p = 0.45$, $\rho = 0.163$, $d = 0.5$, $k_1 = 1.3$ and $k_2 = -0.2$.

in principle by the first stability index (33), given by

$$\sigma_{1PD} = \frac{1}{p + 1 - \dfrac{k_1 d}{(2-d)^2}} \left[\frac{-1}{p - 1 - \dfrac{k_1}{2-d}} + \frac{8k_2}{(2-d)^3} \right]. \tag{40}$$

The index σ_{1PD} vanishes when $p_o = 1 + k_1/(2-d) + (2-d)^3/(8k_2)$. Since this indicates the existence of degenerate period-doubling bifurcations, the second stability index has to be calculated in order to determine the properties of the emerging orbit(s). Then, compute (34) at the degeneracy,

$$\sigma_{2PDO} = \frac{-1}{2\left[p_o + 1 - \dfrac{k_1 d}{(2-d)^2}\right]\left[p_o - 1 - \dfrac{k_1}{2-d}\right]^3}.$$

Now, if k_1 is arbitrary, $k_2 < 0$ and $p_o \in (-1 + k_1 d/(2-d)^2, 1 + k_1/(2-d))$, it is found that $\sigma_{2PDO} > 0$, i.e. a stable period-two orbit arises at the degeneracy. In addition, the sign of σ_{2PD} holds for any combination of the parameters in the surrounding singularity. Therefore, a unique stable orbit appears for $p_o < p < 1 + k_1/(2-d)$ ($\sigma_{1PD} > 0$) while both stable and unstable period-two points are detected for $-1 + k_1 d/(2-d)^2 < p < p_o$ ($\sigma_{1PD} < 0$).

A similar procedure can be carried out for invariant orbits emerging from Hopf bifurcations, but due to the extension of their expressions, only its numerical results together with those obtained for period-doubling bifurcations will be shown. Figure 6 depicts the saddle-node (SN), period-doubling (PD) and Hopf (HB) bifurcation curves when $k_1 = 1.3$, $k_2 = -0.2$, $d = 0.5$ and p and ρ are chosen as the bifurcation parameters. The curves for period-doubling and Hopf bifurcations have an indication of the sign of the first stability index for completeness. In the figure, the strong resonances are indicated as B, C, D and E for the 1:1, 1:4, 1:3 and 1:2 cases, respectively. Notice that the points B and E can also be seen as the intersections between HB and SN curves and HB and PD curves, respectively. Point A represents a singularity related to the interaction between the SN and PD curves. A detailed description of the different dynamics around it can be found in [D'Amico *et al.*, 2003a] and also in [Shilnikov *et al.*, 2001], considering a kind of perturbed Hénon map but without control.

The degenerate period-doubling ($\sigma_{1PD} = 0$) and degenerate Hopf ($\sigma_{1HB} = 0$) conditions occurring at the points $(\rho_{DO}, p_{DO}) = (4.0634, -0.2427)$ and $(\rho_{HO}, p_{HO}) = (0.1699, 0.4156)$, respectively, are also included in Fig. 6. Moreover, numerical simulations within these points have been performed to corroborate the theoretical results. For period-doubling bifurcations, the computations look qualitatively identical to the ones reported in the previous example so, for the sake of conciseness, they will be omitted here. For Hopf bifurcations, since it is found that $\sigma_{2HB} < 0$ for small perturbations around (ρ_{HO}, p_{HO}), the single invariant orbits are obtained when $\sigma_{1HB} < 0$ ($p > p_{HO}$), contrary to the period-doubling case. Furthermore, these solutions are unstable. Figure 7 illustrates this phenomenon considering $p = 0.45$ and $\rho = 0.163$. On the other hand, multiple orbits arise from the critical Hopf curve when $\sigma_{1HB} > 0$ ($p < p_{HO}$). The

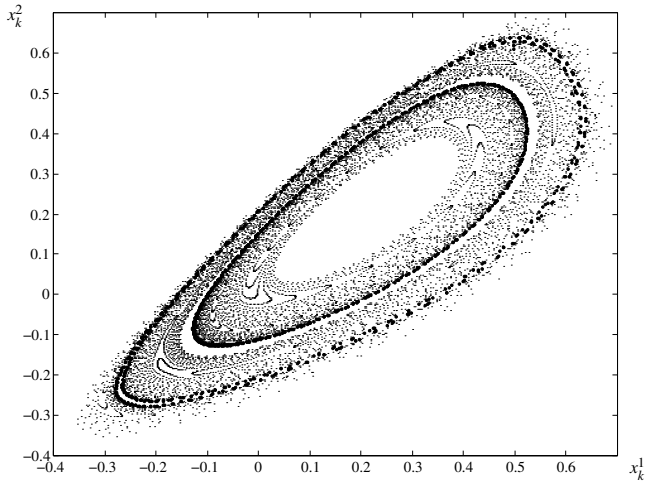

Fig. 8. Dynamical behavior of the controlled Hénon map for $p = 0.38$, $\rho = 0.1794$, $d = 0.5$, $k_1 = 1.3$ and $k_2 = -0.2$. Two invariant orbits can be observed: the inner orbit is stable and the outer is unstable.

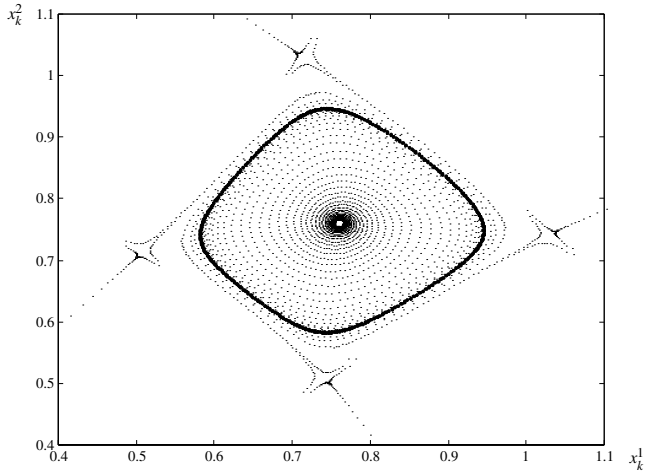

Fig. 9. Dynamical behavior of the controlled Hénon map near the strong 1:4 resonance point C indicated in Fig. 6. The parameter values are $p = -0.475$, $\rho = 1.698$, $d = 0.5$, $k_1 = 1.3$ and $k_2 = -0.2$.

unstable and stable orbits interacting with the unstable fixed point are shown in Fig. 8 for $p = 0.38$ and $\rho = 0.1794$.

To complete the picture, the dynamical behavior of the controlled Hénon map near the singular points C (strong 1:4 resonance) and D (strong 1:3 resonance) is depicted in Figs. 9 and 10, respectively. In both cases, the stable invariant orbits are surrounded by a number of saddle-node points. These points correspond to an unstable periodic orbit in which the period depends on the kind of strong resonance. It is worth mentioning that these

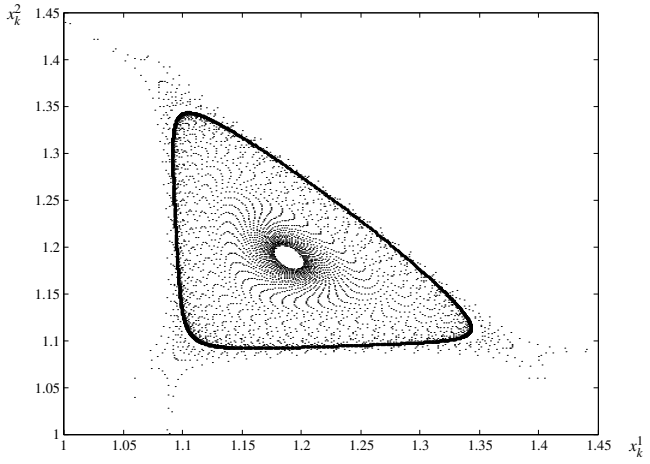

Fig. 10. Dynamical behavior of the controlled Hénon map near the strong 1:3 resonance point D indicated in Fig. 6. The parameter values are $p = -0.618$, $\rho = 3.338$, $d = 0.5$, $k_1 = 1.3$ and $k_2 = -0.2$.

figures are, indeed, related to one of the several typical complex bifurcation sets that can appear in a neighborhood of strong resonance singularities [Kuznetsov, 1995].

5. Conclusions

A unified methodology using a feedback systems representation and the harmonic balance method has been used to detect some degeneracies of period-doubling and Hopf bifurcations in maps. The formulation, also known as the frequency-domain approach due to its input–output properties and its dependence on the frequency response, parallels previous results arising in degenerate Hopf bifurcations in continuous-time nonlinear feedback systems. Although the period-doubling and Hopf degeneracies seem to be very particular and localized in the parameter setting, their effects are actually noticeable in vast regions of the parameter space. As was shown, they can involve the appearance of saddle-node bifurcations in the period-two branch or in the invariant cycle branch, respectively. An approximation using fourth-order harmonic balance has been demonstrated to capture the essential dynamics in the unfoldings of both degeneracies properly. The present technique is powerful since there is no need to reduce the dynamics to the center manifold nor to perform a change of coordinates such as in other classical methods. Furthermore, the approach has profound roots in control theory and thus its fundaments are

very familiar to electrical, mechanical and chemical engineers.

Acknowledgments

The authors acknowledge the support from Consejo Nacional de Investigaciones Científicas y Técnicas (CONICET) and Secretaría General de Ciencia y Tecnología at the Universidad Nacional del Sur.

References

Abed, E. H., Wang, H. O. & Chen, R. C. [1994] "Stabilization of period doubling bifurcations and implications for control of chaos," *Physica* **D70**, 154–164.

Aroudi, A. E., Benadero, L., Toribio, E. & Olivar, G. [1999] "Hopf bifurcation and chaos from torus breakdown in a PWM voltage-controlled DC–DC boost converter," *IEEE Trans. Circuits Syst.-I: Fund. Th. Appl.* **46**, 1374–1382.

Chenciner, A. [1985] "Bifurcations de points fixes elliptiques II. Orbites périodiques et ensembles de Cantor invariants," *Invent. Math.* **80**, 81–106.

D'Amico, M. B., Moiola, J. L. & Paolini, E. E. [2002] "Hopf bifurcation for maps: A frequency-domain approach," *IEEE Trans. Circuits Syst.-I: Fund. Th. Appl.* **49**, 281–288.

D'Amico, M. B., Moiola, J. L. & Paolini, E. E. [2003a] "Controlling bifurcations in maps via a frequency-domain approach," *Dyn. Contin. Discr. Impuls. Syst. Ser. B Appl. Algorithms* **10**, 781–798.

D'Amico, M. B., Moiola, J. L. & Paolini, E. E. [2003b] "Stability analysis of degenerate Hopf bifurcations for discrete-time systems," *Latin Amer. Appl. Res.* **33**, 413-418.

Deane, J. H. B. & Hamill, D. C. [1990] "Instability, subharmonics, and chaos in power electronic systems," *IEEE Trans. Power Electron.* **5**, 260–268.

di Bernardo, M. & Vasca, F. [2000] "Discrete-time maps for the analysis of bifurcations and chaos in DC/DC converters," *IEEE Trans. Circuits Syst.-I: Fund. Th. Appl.* **47**, 130–142.

Dilão, R. & Domingos, T. [2001] "Periodic and quasi-periodic behavior in resource-dependent age structured population models," *Bull. Math. Biol.* **63**, 207–230.

Frouzakis, C. E., Adomaitis, R. A. & Kevrekidis, I. G. [1991] "Resonance phenomena in an adaptively-controlled system," *Int. J. Bifurcation and Chaos* **1**, 83–106.

Frouzakis, C. E., Adomaitis, R. A. & Kevrekidis, I. G. [1996] "An experimental and computational study of subcriticality, hysteresis and global dynamics for a model adaptive control system," *Comput. Chem. Eng.* **20**, S1029–S1034.

Golden, M. P. & Ydstie, B. E. [1988] "Bifurcation in model reference adaptive control systems," *Syst. Contr. Lett.* **11**, 413–430.

Itovich, G. R. & Moiola, J. L. [2002] "Characterization of dynamic bifurcations in the frequency domain," *Int. J. Bifurcation and Chaos* **12**, 87–101.

Kuznetsov, Y. A. [1995] *Elements of Applied Bifurcation Theory* (Springer-Verlag, NY).

Mareels, I. M. Y. & Bitmead, R. R. [1988] "Non-linear dynamics in adaptive control: Periodic and chaotic stabilization–II. Analysis," *Automatica* **24**, 485–497.

Mazumder, S. K., Nayfeh, A. H. & Boroyevich, D. [2001] "Theoretical and experimental investigation of the fast- and slow-scale instabilities of a DC–DC converter," *IEEE Trans. Power Electron.* **16**, 201–215.

Mees, A. I. & Chua, L. O. [1979] "The Hopf bifurcation theorem and its applications to nonlinear oscillations in circuits and systems," *IEEE Trans. Circuits Syst.* **CAS-26**, 235–254.

Moiola, J. L. & Chen, G. [1996] *Hopf Bifurcations Analysis: A Frequency Domain Approach* (World Scientific, Singapore).

Peckham, B. B. & Kevrekidis, I. G. [1991] "Period doubling with higher-order degeneracies," *SIAM J. Math. Anal.* **22**, 1552–1574.

Peckham, B. B., Frouzakis, C. E. & Kevrekidis, I. G. [1995] "Bananas and banana splits: A parametric degeneracy in the Hopf bifurcation for maps," *SIAM J. Math. Anal.* **26**, 190–217.

Selgrade, J. F. & Roberds, J. H. [1997] "Period doubling bifurcations for systems of difference equations and applications to models in population biology," *Nonlin. Anal.* **29**, 185–199.

Shilnikov, L. P., Shilnikov, A. L., Turaev, D. V. & Chua L. O. [2001] *Methods of Qualitative Theory in Nonlinear Dynamics. Part II* (World Scientific, Singapore).

Tse, C. K. [1994] "Flip bifurcation and chaos in three-state boost switching regulators," *IEEE Trans. Circuits Syst.-I: Fund. Th. Appl.* **41**, 16–23.

Tse, C. K., Lai, Y. M. & Iu, H. H. C. [2000] "Hopf bifurcation and chaos in a free-running current-controlled Cuk switching regulator," *IEEE Trans. Circuits Syst.-I: Fund. Th. Appl.* **47**, 448–457.

Wen, G., Xu, D. & Han, X. [2002] "On creation of Hopf bifurcations in discrete-time nonlinear systems," *Chaos* **12**, 350–355.

Appendix

The second-order approximation of an orbit emerging from a period-doubling bifurcation is given by $y_k^D = \hat{y} + Y_0^D + Y_1^D e^{i\pi k}$, with

$$Y_0^D = V_{02}^D \theta^2 \,,$$

$$Y_1^D = V_{11}^D \theta + V_{13}^D \theta^3 \,.$$

The necessary formulas for computing the previous coefficient vectors are

$$V_{02}^D = -\frac{1}{2} H(1;\mu) D_2 f(\hat{y};\mu)(V_{11}^D)^2 \,,$$

and

$$P_D[I + G(-1;\mu)J(\mu)]V_{13}^D = -P_D G(-1;\mu)W_{13}^D \,,$$

under the constraint $V_{13}^D \perp V_{11}^D$ and with

$$W_{13}^D = D_2 f(\hat{y};\mu)V_{11}^D V_{02}^D + \frac{1}{6} D_3 f(\hat{y};\mu)(V_{11}^D)^3 \,.$$

Now, considering a fourth-order harmonic balance, the coefficients Y_0^D and Y_1^D are transformed into the expressions

$$\begin{aligned} Y_0^D &= V_{02}^D\theta^2 + V_{04}^D\theta^4 \,, \\ Y_1^D &= V_{11}^D\theta + V_{13}^D\theta^3 + V_{15}^D\theta^5 \,, \end{aligned}$$

where remaining vectors can be calculated as

$$\begin{aligned} V_{04}^D = -\frac{1}{2} H(1;\mu)\{ & D_2 f(\hat{y};\mu)[2V_{11}^D V_{13}^D + (V_{02}^D)^2] \\ & + D_3 f(\hat{y};\mu)(V_{11}^D)^2 V_{02}^D \\ & + \frac{1}{12} D_4 f(\hat{y};\mu)(V_{11}^D)^4\} \,, \end{aligned}$$

and

$$P_D[I + G(-1;\mu)J(\mu)]V_{15}^D = -P_D G(-1;\mu)W_{15}^D \,,$$

with

$$\begin{aligned} W_{15}^D = {} & D_2 f(\hat{y};\mu)(V_{02}^D V_{13}^D + V_{11}^D V_{04}^D) \\ & + \frac{1}{2} D_3 f(\hat{y};\mu)[V_{11}^D (V_{02}^D)^2 + (V_{11}^D)^2 V_{13}^D] \\ & + \frac{1}{6} D_4 f(\hat{y};\mu)(V_{11}^D)^3 V_{02}^D \\ & + \frac{1}{120} D_5 f(\hat{y};\mu)(V_{11}^D)^5 \,, \end{aligned}$$

and also under the constraint $V_{15}^D \perp V_{11}^D$.

On the other hand, the second-order approximation for Hopf bifurcations is obtained as $y_k^H = \hat{y} + Y_0^H + Y_1^H e^{i\omega k} + Y_2^H e^{i2\omega k}$, where

$$\begin{aligned} Y_0^H &= V_{02}^H\theta^2 \,, \\ Y_1^H &= V_{11}^H\theta + V_{13}^H\theta^3 \,, \\ Y_2^H &= V_{22}^H\theta^2 \,. \end{aligned}$$

In this case, the expression of the coefficient vectors are

$$V_{02}^H = -\frac{1}{4} H(1;\mu) D_2 f(\hat{y};\mu) V_{11}^H \overline{V}_{11}^H \,,$$

$$V_{22}^H = -\frac{1}{4} H(e^{i2\omega};\mu) D_2 f(\hat{y};\mu)(V_{11}^H)^2 \,,$$

and

$$P_H[I + G(e^{i\omega};\mu)J(\mu)]V_{13}^H = -P_H G(e^{i\omega};\mu)W_{13}^H$$

with "$\overline{(\cdot)}$" as the complex conjugate operator and

$$\begin{aligned} W_{13}^H = {} & D_2 f(\hat{y};\mu)\left(V_{11}^H V_{02}^H + \frac{1}{2}\overline{V}_{11}^H V_{22}^H\right) \\ & + \frac{1}{8} D_3 f(\hat{y};\mu)(V_{11}^H)^2 \overline{V}_{11}^H \,. \end{aligned}$$

Again, it is assumed that $V_{13}^H \perp V_{11}^H$.

Based on a fourth-order expansion, the approximated solution can be extended as $y_k^H = \hat{y} + Y_0^H + Y_1^H e^{i\omega k} + Y_2^H e^{i2\omega k} + Y_3^H e^{i3\omega k} + Y_4^H e^{i4\omega k}$, where now

$$\begin{aligned} Y_0^H &= V_{02}^H\theta^2 + V_{04}^H\theta^4 \,, \\ Y_1^H &= V_{11}^H\theta + V_{13}^H\theta^3 + V_{15}^H\theta^5 \,, \\ Y_2^H &= V_{22}^H\theta^2 + V_{24}^H\theta^4 \,, \\ Y_3^H &= V_{33}^H\theta^3 + V_{35}^H\theta^5 \,, \\ Y_4^H &= V_{44}^H\theta^4 \,, \end{aligned}$$

and the remaining vectors are given by

$$\begin{aligned} V_{04}^H = -\frac{1}{4} H(1;\mu)\Big\{ & D_2 f(\hat{y};\mu)[2(V_{02}^H)^2 + V_{11}^H\overline{V}_{13}^H + \overline{V}_{11}^H V_{13}^H + V_{22}^H\overline{V}_{22}^H] \\ & + \frac{1}{4} D_3 f(\hat{y};\mu)[4V_{11}^H\overline{V}_{11}^H V_{02}^H + (V_{11}^H)^2\overline{V}_{02}^H + (\overline{V}_{11}^H)^2 V_{02}^H] + \frac{1}{16} D_1^4 f(\hat{y};\mu) V_{11}^2 \overline{V}_{11}^2\Big\}, \end{aligned}$$

$$\begin{aligned} V_{24}^H = -\frac{1}{4} H(e^{i2\omega};\mu)\Big\{ & 2D_2 f(\hat{y};\mu)[2V_{02}^H V_{22}^H + V_{11}^H V_{13}^H + \overline{V}_{11}^H V_{33}^H] \\ & + D_3 f(\hat{y};\mu)[(V_{11}^H)^2 V_{02}^H + V_{11}^H\overline{V}_{11}^H V_{22}^H] + \frac{1}{12} D_4 f(\hat{y};\mu)(V_{11}^H)^3\overline{V}_{11}^H\Big\}, \end{aligned}$$

$$V_{33}^H = -\frac{1}{4}H(e^{i3\omega};\mu)\left[2D_2f(\hat{y};\mu)V_{11}^H V_{22}^H + \frac{1}{6}\,D_3f(\hat{y};\mu)(V_{11}^H)^3\right],$$

$$V_{44}^H = -\frac{1}{4}H(e^{i4\omega};\mu)\Big\{D_2f(\hat{y};\mu)[2V_{11}^H V_{33}^H + (V_{22}^H)^2] + \frac{1}{2}\,D_3f(\hat{y};\mu)(V_{11}^H)^2 V_{22}$$
$$+ \frac{1}{48}\,D_4f(\hat{y};\mu)(V_{11}^H)^4\Big\},$$

$$V_{35}^H = -\frac{1}{4}H(e^{i3\omega};\mu)\Big\{2D_2f(\hat{y};\mu)(2V_{02}^H V_{33}^H + V_{13}^H V_{22}^H + \overline{V}_{11}^H V_{44}^H)$$
$$+ \frac{1}{8}\,D_3f(\hat{y};\mu)[4V_{11}^H V_{02}^H V_{22}^H + (V_{11}^H)^2 V_{13}^H + 2V_{11}^H \overline{V}_{11}^H V_{13}^H + \overline{V}_{11}^H (V_{22}^H)^2]$$
$$+ \frac{1}{16}\,D_4f(\hat{y};\mu)\left[\frac{2}{3}(V_{11}^H)^3 V_{02}^H + (V_{11}^H)^2 \overline{V}_{11}^H V_{22}^H\right] + \frac{1}{384}\,D_5f(\hat{y};\mu)(V_{11}^H)^4 \overline{V}_{11}^H\Big\}$$

and

$$P_H[I + G(e^{i\omega};\mu)J(\mu)]V_{15}^H = -P_H G(e^{i\omega};\mu)W_{15}^H\,,$$

with

$$W_{15}^H = \frac{1}{2}\,D_2f(\hat{y};\mu)(2V_{02}^H V_{13}^H + 2V_{11}^H V_{04}^H + \overline{V}_{11}^H V_{24}^H + \overline{V}_{13}^H V_{22}^H)$$
$$+ \frac{1}{8}\,D_3f(\hat{y};\mu)[4V_{11}^H (V_{02}^H)^2 + 4V_{02}^H \overline{V}_{11}^H V_{22}^H + (V_{11}^H)^2 \overline{V}_{13}^H + 2V_{11}^H \overline{V}_{11}^H V_{13}^H$$
$$+ 2V_{11}^H V_{22}^H \overline{V}_{22}^H + (\overline{V}_{11}^H)^2 V_{33}] + \frac{1}{48}\,D_4f(\hat{y};\mu)[6(V_{11}^H)^2 \overline{V}_{11}^H V_{02}^H + (V_{11}^H)^3 \overline{V}_{22}^H$$
$$+ 3V_{11}^H (\overline{V}_{11}^H)^2 V_{22}^H] + \frac{1}{192}\,D_5f(\hat{y};\mu)(V_{11}^H)^3 (\overline{V}_{11}^H)^2\,,$$

under the constraint $V_{15}^H \perp V_{11}^H$.